Journal of Extracellular Biology

RESEARCH ARTICLE OPEN ACCESS

Extracellular Vesicles From Follicular Fluid in Infertile Women: Size, Morphology and miRNA Content Analysis

Solène Ducarre[1,2] | Regina Maria Chiechio[1,3] | Gregory Moulin[4] | Ester Butera[1,5] | Aurélien Dupont[6] | Christophe Penno[7,8] | Abdelhak El Amrani[7] | Claire Heichette[6] | Pascale Even-Hernandez[1] | Valérie Marchi[1] | Célia Ravel[2,4]

[1]Institut des Sciences Chimiques de Rennes ISCR UMR CNRS 6226, Université de Rennes, Rennes, France | [2]Inserm, EHESP, Irset (Institut de Recherche en Santé, Environnement et Travail) – UMR_S 1085, Université de Rennes, Rennes, France | [3]Dipartimento di Fisica e Astronomia, Università di Catania, Catania, Italy | [4]CHU Rennes, Service de Biologie de la Reproduction-CECOS, Rennes, France | [5]Dipartimento di scienze chimiche, Università di Catania, Catania, Italy | [6]UMR6 UMS 3480, US_S 018, BIOSIT, Univ. Rennes, CNRS, Inserm, Rennes, France | [7]ECOBIO UMR 6553 CNRS, Université de Rennes, Rennes, France | [8]APC Microbiome Ireland, University College Cork, Cork, Ireland

Correspondence: Célia Ravel (celia.ravel@chu-rennes.fr)

Received: 13 September 2024 | **Revised:** 31 January 2025 | **Accepted:** 15 February 2025

Funding: The authors received no specific funding for this work.

Keywords: extracellular vesicles (EVs) | polycystic ovarian syndrome (PCOS) | diminished ovarian reserve (DOR) | follicular fluid (FF) | morphology | Cryo-TEM | miRNA

ABSTRACT

The declining birth rates and fertility challenges in Europe have intensified global concerns over rising infertility, particularly among women. This study decisively investigates follicular fluid-related extracellular vesicles (FF-EVs) from infertile patients with polycystic ovary syndrome (PCOS) or diminished ovarian reserve (DOR) undergoing in vitro fertilization (IVF), comparing them to a healthy control group. We have identified significant variations in protein content and polydispersity in crude follicular fluid using UV-Vis absorption and dynamic light scattering (DLS) techniques. Furthermore, the morphology of the extracellular vesicles (EVs) and the patterns of non-coding RNA content, including miRNAs, reveal distinct differences in infertile patients. These findings offer critical insights into the molecular signatures associated with these conditions. This study plays a vital role in advancing reproductive healthcare by pinpointing potential targets that can enhance diagnosis and deepen our understanding of ovarian disorders.

1 | Introduction

Human infertility is on the rise globally, presenting societal challenges and significant public health concerns (Aitken 2024). One cause of female infertility concerns ovarian dysfunction. Any imbalance in the number of germ cells within the ovaries may lead to an atypical process known as autophagy-assisted phagocytosis and ineffective elimination of apoptotic oocytes by granulosa cells (Yefimova et al. 2020). This dysfunction can result in pathological conditions such as polycystic ovarian syndrome (PCOS) or diminished ovarian reserve (DOR).

An excessive ovarian function characterized by an abnormally high development of follicles leads to PCOS (Azziz et al. 2016; Ehrmann 2005; Joham et al. 2022). PCOS is the most common endocrine disorder among reproductive-aged women (Goodman et al. 2015a, 2015b). The diagnosis of PCOS is made through the presence of polycystic ovaries observed in ultrasound examinations combined with additional factors such as menstrual

abnormalities and anovulation (Ehrmann 2005). The clinical presentation of this syndrome is associated with androgen excess and insulin resistance, which can result in reproductive difficulties. PCOS has a hereditary component influenced by epigenetic factors (Mimouni et al. 2021).

Conversely, ovarian dysfunction can lead to follicle exhaustion and DOR, defined as the number of oocytes remaining in the ovary, resulting in ovarian failure (Ravel et al. 2016). DOR patients present a diminished follicle number as compared to control patients of the same age (Cohen et al. 2015).

In both types of ovarian dysfunction, hormone secretion is disrupted. This affects gonadotropins and also alters the secretion of Anti-Mullerian Hormone (AMH), which is typically elevated in patients with PCOS and significantly reduced in those with DOR (Cedars 2022). AMH levels appear to be a more sensitive marker of ovarian reserve compared with early follicular-phase hormone levels (Penzias et al. 2020).

Follicular fluid (FF) is produced by granulosa cells during the development of the follicular antrum. This fluid is rich in EVs, which vary significantly in size and morphology (Neyroud et al. 2022). EVs play a crucial role as regulators in ovarian pathophysiology. Research has shown that these EVs are absorbed by the immature cumulus-oocyte complex (COC) delivering their membrane proteins and lipids to the COCs (de Almeida Monteiro Melo Ferraz et al. 2020). The proteins found in follicular fluid-related extracellular vesicles (FF-EVs) may have important functions in modulating the resumption of meiosis, including roles in cumulus cell expansion, nuclear envelope breakdown and spindle stabilization. Labelled EVs have been observed outside the transzonal projections formed by the cytoplasmic extensions of cumulus cells, which are present during the early stages of oocyte maturation. These EVs can mediate the transfer of RNA molecules between cumulus cells and the oocyte, suggesting that cell-secreted vesicles are released into the perivitelline space (Macaulay et al. 2014). However, the specific content of these EVs with respect to the ovarian physiological state is still not fully understood. Recent studies have highlighted the significant role of FF-derived microRNAs (miRNAs) in regulating the functions of ovarian cells (Wang et al. 2023; Zhao et al. 2022).

In this study, we compare FF-EVs from infertile patients with PCOS or DOR to those from healthy donors. To identify key features associated with FF-EVs specific to infertile women, we investigate their morphology, size and miRNA content, as well as the protein content in the crude FF. This work reveals pioneering molecular signatures relevant for ovarian physiology and can serve as a basis for future research directions.

2 | Materials and Methods

2.1 | Study Design and Subjects

The study involved French women aged 20 to 40. Samples were collected at the ART centre CECOS of Rennes University Hospital (CHU de Rennes) through the GERMETHEQUE biobank, which is dedicated to human fertility. All couples provided informed consent before using a sample of FF from the oocyte retrieval process as part of the IVF procedure. Additionally, ethical permission (CP-GM n°20220705) was obtained for this study. Patients underwent stimulation using an antagonist protocol with recombinant FSH. Thirty-six hours after receiving an injection of 10,000 IU of human chorionic gonadotropin (hCG) and after at least three ovarian follicles had reached a diameter of 18 mm, the follicles were aspirated. FF samples were obtained from 72 healthy, normally ovulating patients who underwent intracytoplasmic sperm injection due to male factor infertility, 48 patients with DOR and 48 patients with PCOS. The key factors differentiating ovarian physiology among these groups were the AMH level and antral follicle count (AFC) (Cedars 2022). The average age of normo-ovulating patients was 33.2 years, with an average AFC of 21.4 and an average AMH level of 3.17 ng/mL. In contrast, the average age of DOR patients was 31.1 years, with a diminished average AFC of 10.9 and an average AMH level of 1.02 ng/mL. The average age of PCOS patients was 31.5 years, with an increased average AFC of 46 and an average AMH level of 5.72 ng/mL.

2.2 | Follicular Fluid Collection, Storage Conditions and EVs Purification

FF was collected through transvaginal ultrasound-guided aspiration of follicles measuring up to 18 mm in diameter. The fluid samples were centrifuged at 1600 × *g* for 10 min at 4°C to remove cellular components, and the supernatant was stored at −80°C. Before analysis, the samples were thawed at room temperature and centrifuged again at 800 × *g* for 20 min to eliminate large aggregates. For ultraviolet-visible (UV-Vis) and dynamic light scattering (DLS) analyses, the crude FF was used as is. The samples were further purified according to the specific technique employed (see Figure 1). A summary of the preparation of all EV samples is provided in Table S1 (Supplementary Material). All samples were prepared in accordance with the MISEV guidelines (Welsh et al. 2024; Théry et al. 2018).

2.3 | Cryo-Transmission Electron Microscopy (Cryo-TEM)

For Cryo-TEM analysis, the sample from healthy participants consisted of a pool of 16 FF samples from normo-ovulating patients. The DOR sample was derived from a pool of 8 FF from DOR patients, while the PCOS sample included a pool of 8 FF from PCOS patients. To increase the sample concentration, ultracentrifugation (UC) was performed at 4°C at 100,000 × *g* for 90 min. Each pellet was then re-suspended in 250 µL of PBS buffer just before preparing the CryoTEM grids. The samples were vitrified using an automatic plunge freezer (EM GP, Leica) with regulated temperature and humidity, as described by (Dubochet et al. 1988). They were placed on glow-discharged electron microscope grids and quickly frozen in liquid ethane, followed by blotting and vitrification. A 200 kV electron microscope (Tecnai G2 T20 Sphera, FEI) equipped with a 4k × 4k CCD camera (TemCam-XF-416, TVIPS) was used to monitor the grids after they were transferred to a single-axis cryo-holder (model 626, Gatan). Micrographs were taken at a nominal magnification of 25,000×, with the camera set to binning mode 1 and under low electron doses. The diameter of 2138 EVs from the captured images were

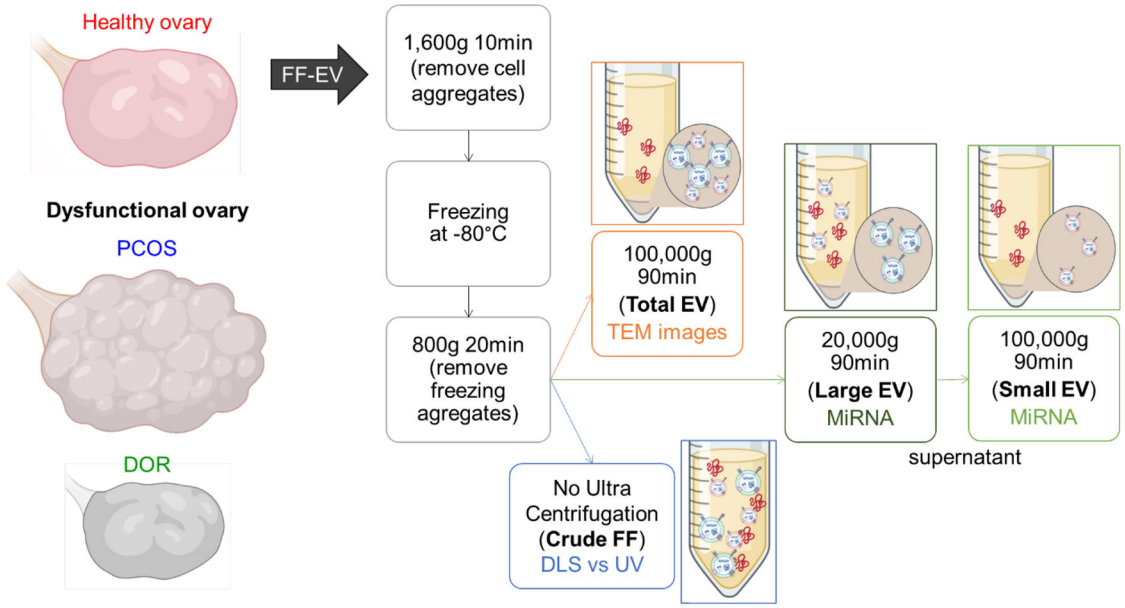

FIGURE 1 | Isolation and purification of EVs from human follicular fluid (crude FF, total EVs, large EVs and small EVs).

measured and categorized into nine subcategories based on a modified classification (Höög and Lötvall 2015) according to their diameter and morphology. A total of 63 images were analysed, revealing 593 EVs in the DOR group, 656 EVs in the PCOS group from 74 images and 889 EVs in the control group from 78 images.

2.4 | Dynamic Light Scattering (DLS)

DLS experiments were conducted using individual FF samples (assay 1) or pools containing four patients (assay 2) with the same pathology to highlight the specific effects of each ovarian condition. For each group, the population was further divided into two age categories: 21–30 years old and 31–40 years old. After FF collection, the samples were ready for use without any additional purification. The hydrodynamic diameters were measured using a Nanosizer ZEN3600 (Malvern Instruments, England), without diluting the samples. Measurements were taken at a scattering angle of 173° and at a temperature of 25°C. The mean scattering intensity is given in unit kilocount of photons per second (Kcps) corresponding to the average number of photons per second reaching the detector.

2.5 | UV-Vis Spectrometer

Absorbance experiments were conducted on individual FF samples (assay 1) as well as pooled samples from four patients (assay 2) with the same phenotype to highlight the specific effects of each ovarian pathology. A Thermo Scientific NanoDrop UV-Vis spectrometer was used to obtain absorbance spectra, with each sample diluted ten times using PBS buffer.

2.6 | Nanoparticle Tracking Analysis (NTA)

Samples were diluted with PBS by a 10-fold factor before measurement on a NanoSight LM10 unit (Malvern Instruments, Malvern, UK). For size distribution and concentration measurements, three videos of 30 s were recorded for each sample at 25°C, ensuring that the number of tracks analysed was at least 200. The videos were then analysed using NanoSight NTA 3.1 software (Malvern, UK), which provided high-resolution particle size distribution profiles and concentration measurements of the vesicles in solution.

2.7 | RNA Purification

Each sample was obtained from a pool of four patients, taking into account the ovarian phenotype (Healthy, DOR and PCOS) and age groups (21–30 and 31–40 years) after FF collection. The samples were then ultracentrifuged at 20,000 × *g* for 90 min. The pellet was resuspended in 250 µL of PBS buffer (large EVs), and the supernatant was further ultracentrifuged at 100,000 × *g* for another 90 min. The resulting pellet was again resuspended in 250 µL of PBS buffer (small EVs). Total RNA isolation from purified EVs, including microRNAs, was performed using the miRNeasy Micro Kit 50 (Qiagen, reference 217084), following the manufacturer's instructions. For this process, 100 µL of the purified vesicles, stored in 1X PBS at −80°C, was used as the starting material and mixed with 700 µL of QIAzol in a 2 mL BeadBug tube prefilled with 0.1 mm silica glass beads that had been acid-washed (Sigma, reference Z763721). The tubes were agitated at 30 ms^{-1} for 1 min using bead beating. The subsequent steps of RNA isolation adhered to the Quick-Start Protocol provided by Qiagen. The RNA was eluted in 15 µL of RNase-free water. An aliquot of 4 µL was transferred to an RNase-free microtube for RNA quality control, while the remaining 10 µL volume was immediately stored at −80°C.

2.8 | RNA Analysis

The integrity and size distribution of RNA extracted from EVs were analysed using the Agilent 2000 Bioanalyzer (Agilent

Technologies). We employed an Agilent RNA 6000 Pico kit, which allows for qualitative analysis of RNA size distribution ranging from 25 nucleotides (nt) to 6000 nt. Additionally, we utilized an Agilent small RNA kit to conduct a more detailed assessment of small RNAs, with sizes ranging from 4 to 150 nt. The analysis was performed using 1 μL of purified RNA, following the manufacturer's instructions.

2.9 | RNA Sequencing

Library preparation and sequencing were conducted by Helixio. A total of 1 ng of RNA was used to prepare the NGS library using the D-Plex Small RNA-seq and D-Plex Unique Dual Indexes kits from Diagenode, following the manufacturer's protocol. The libraries were then purified with the MicroChIP DiaPure kit (Diagenode) and subsequently with Agencourt AMPure XP magnetic beads, without any size selection. The quality and quantity of the library were analysed using the Bioanalyser 2100 and the Agilent Technologies plate assay. Twelve libraries were sequenced on an Illumina NextSeq 500 platform using 75 nt single-end sequencing. The average sequencing depth for each library was approximately 15.5 million NGS reads.**Bioinformatics Analysis:** The quality of the reads was assessed using FastQC. Sequence adaptors and rRNA contamination were removed with BBMap and filtered using Cutadapt. After filtering, the reads were mapped to the human reference genome from Ensembl GRCh38 release 108 using the STAR aligner. The reads were then counted with HTSeq software, specifically the htseq-count module, which counts the number of reads aligned to intervals defined in a reference file. These intervals correspond to the transcripts annotated in the Ensembl transcriptome. The mode used in this analysis accounted for reads that were aligned multiple times and required a MAPQ mapping score of at least 10.

A descriptive analysis was performed on the total filtered small RNA using the Bioconductor DESeq2 package, resulting in 1913 small RNAs with at least 10 reads across all samples. Following this, differential analysis was conducted using the EdgeR package. Small RNAs that were deemed differentially expressed were identified based on a corrected p-value of less than 0.05, applying the Benjamini-Hochberg correction method.

2.10 | Target Gene Predictions and Pathway Analysis

DIANA miRPath v4.0 was used to conduct in silico union pathway analysis for the selected miRNAs. These miRNAs were identified through a Venn diagram, with each category having an average of more than 10 reads and grouped by fold change. For the pathway analysis, only significant results were plotted ($p < 0.05$).

3 | Results and Discussion

The goal of this study was to identify the distinguishing physicochemical parameters that differentiate EVs from healthy individuals and those from patients with either ovarian hyperactivity (PCOS) or hypoactivity (DOR). These parameters included the size, polydispersity, morphology, and miRNA content of the EV population, as well as the protein content in the FF. This information provides valuable insights into the characterization of PCOS and DOR pathologies.

This study was the first to explore the relationship between morphology and content of FF-EVs, an aspect that has not been thoroughly investigated before. To assess the impact of ovarian function on FF-derived EVs, we analysed three types of samples (see Figure 1). We optimized the treatment of FF samples for each analysis technique to isolate the EVs and classify them into two subpopulations based on size, as illustrated in Figure 1.

For Cryo-TEM, we examined the total population of EVs. However, for miRNA content analysis, we focused on two subpopulations, as the miRNA content is known to correlate with EV size. To achieve this, a first UC step at 20,000 × g was performed on the samples to separate the "large EVs," which are thought to contain microvesicles, from the "small EVs," which are separated using a second UC step at 100,000 × g, containing exosomes (Lischnig et al. 2022).

The crude FF sample was not treated with UC steps to preserve the original composition and size of its content, thus minimizing potential artefacts from excessive sample manipulation during DLS and UV spectroscopy. However, UC was utilized to enrich the sample in EVs for Cryo-TEM imaging and the analysis of miRNA content, as summarized in Table S1.

3.1 | Size and Protein Content Analysis of the Crude Follicular Fluid

The size distribution of EVs in crude FF was first analysed using DLS techniques. Given the high polydispersity of the samples, we directly compared the correlograms across different phenotypes and patient age groups. This comparison focused on evaluating both the position and the slope of the correlation coefficient function over time. The position of the curve provides a rough estimation of the characteristic mean scattering time, which increases with EV size. In contrast, the slope indicates the polydispersity of the EVs, where a lower slope suggests greater polydispersity. We observed significant differences related to patient age in crude FF. Larger particles were found in older patients (aged 31–40), as evidenced by their higher polydispersity and longer diffusion times (see Figure S1a,b). The age-related effect on polydispersity is less pronounced in patients with DOR, as shown in Figure S1. This could be due to a decrease in the average secretion of EVs with age in this group.

No significant differences in size were detected between the different phenotypes due to the high polydispersity of all the samples. The size distribution of FF-EVs from patients with PCOS was even more polydisperse (polydispersity index, PDI: 0.943 ± 0.037) compared to that of the control group (PDI: 0.826 ± 0.033) and the DOR patients (PDI: 0.784 ± 0.017). In all cases, the characteristic time corresponding to the decay of the autocorrelation function was observed to be within the range of a few hundred microseconds, regardless of the phenotype. Therefore, the DLS technique alone did not allow for differentiation between the different phenotypes.

To complete the data about the EV population in crude FF, we measured the absorbance at 280 nm to quantify the protein content. This wavelength was chosen as a compromise to maximize the contribution of protein absorption versus that of nucleic acid and light scattering. The protein content in crude FF accounts not only for the proteins on the surface of EVs but also for the circulating proteins in the FF, which can be used to assess granulosa cell activity.

We then plotted the absorbance at 280 nm against the DLS count rate for each sample to differentiate between these two parameters. This approach allowed us to rapidly gain valuable insights into the EVs population within the crude FF samples without the need for further treatment.

In our first assay, we analysed 16 individual patients per phenotype (assay 1) and confirmed the significance of the data using Analysis of Variance (ANOVA). The protein absorbance for PCOS patients was 4.84 ± 0.31, which significantly exceeded the average value of 4.37 ± 0.57 for healthy patients ($p = 0.0193$). In contrast, the protein absorbance for DOR patients was within the range of healthy patients (4.26 ± 0.46). However, the concentration and size of EVs for DOR patients deviated significantly from the average. The DLS count rate for DOR patients was 172 ± 33 kcps, compared to 220 ± 8 kcps for healthy patients ($p = 0.0004$). In comparison, PCOS patients exhibited normal EV concentration and size, with a DLS count rate of 211 ± 37 kcps. These results indicate that the protein content in the samples from PCOS patients is significantly higher compared to healthy patients, despite having similar EV count rates. Furthermore, the DLS count rate for DOR patients was significantly lower than that of both healthy and PCOS patients (see Figure 2a,b).

To evaluate the potential impact of individual patient characteristics on this analysis, pools of four patients were further investigated in a second assay (assay 2). The analysis of the crude FF using UV-visible absorbance and DLS count rate revealed a significant difference between infertile and healthy patients, consistent with the results from assay 1. The concentrations and sizes of EVs, along with their corresponding protein content, were estimated using NTA, DLS and absorbance measurements (see Table S2) for each group. As shown in Figure 2 and Table S2, patients with ovarian hyperactivity (PCOS) had a higher protein content in their crude FF compared to the healthy control group. However, the size and concentration of EVs were similar in both groups. Specifically, the average absorbance at 280 nm for PCOS patients was 4.8 ± 0.2, which is greater than that of the control group at 4.2 ± 0.1 ($p = 0.01324$). The mean DLS count rate for PCOS patients was 182 ± 14 kpcs, similar to the count rate of 179 ± 11 kpcs for healthy patients. Conversely, patients with low ovarian activity (DOR) exhibited lower EV concentrations and smaller EVs compared to healthy patients, along with reduced protein content. The mean absorbance at 280 nm for DOR patients was 3.7 ± 0.8 ($p = 0.01741$), and the mean DLS count rate was 150 ± 13 kpcs ($p = 0.01278$). Furthermore, healthy patients displayed more consistent absorbance and count rate values than the infertile groups, with a standard deviation of 0.1 for absorbance and 5 kpcs for the DLS count rate (see Figure 2c,d). It was not possible to distinguish between PCOS patients and healthy patients based on the DLS count rate alone. Additionally, no discernible impact of patient age was observed when plotting the absorbance against the DLS count rate. However, similar to the AMH levels, DOR patients had lower concentrations of both protein content and vesicles in their samples compared to healthy and PCOS patients, who were above average in these criteria.

These results further emphasized the reliability of the trends observed in the previous assay (see Figure 2 and Figure S2). This analysis demonstrated that protein content, as well as the size and concentration of EVs, are influenced by ovarian physiology. Patients presenting with PCOS characterized by ovarian hyperactivity, exhibited protein levels higher than those of healthy controls, while maintaining a normal concentration of EVs. In contrast, patients with DOR, who exhibit ovarian hypoactivity, had protein content within the normal range but displayed lower concentrations and sizes of EVs. These findings could also enhance our understanding of the underlying processes associated with these pathologies.

3.2 | EV Morphologies and Cryo-TEM Images

To better understand the potential relationship between the morphological distribution of EVs and ovarian physiology, we investigated their morphology using Cryo-TEM. This analysis was conducted after UC to concentrate the EVs in the samples (referred to as total EVs in Figure 1). To explore the diversity of EV morphologies, we utilized a modified classification initially reported for human seminal fluid (Höög and Lötvall 2015) and applied it to FF-EVs of healthy patients in our recent study (Neyroud et al. 2022). This classification system enabled us to categorize and understand the various EV morphologies within the samples. A significant diversity in morphology was observed across the phenotypes, as shown in Figure 3a–c.

However, the systematic morphological classification revealed three notable differences in the distribution of morphologies (Figure 3d). Firstly, unilamellar rounded-shaped vesicles were much more abundant (55.8%) in the group of healthy patients, with only a few vesicles showing deformation, including 9.9% double vesicles. In contrast, EVs from patients with ovarian dysfunction displayed more complex shapes, with only around 38% of simple vesicles in both groups. Secondly, the proportion of oval vesicles was higher in samples from patients with ovarian pathology, accounting for 35.1% for DOR and 35.7% for PCOS patients, compared to 23.5% in healthy controls. Finally, PCOS patients had a significantly higher proportion (4%) of tubular-shaped vesicles, including both small and large tubular structures, which is two times greater than that observed in healthy patients (1.5%) and in DOR patients (1.7%). DOR patients also showed a higher proportion of sacs EV (5.1%) as compared to healthy individuals (1.6%) or PCOS patients (1.4%). These morphological variations can be attributed to ovarian pathology and provide important insights for detection through Cryo-TEM analysis.

We then analysed the EV size in function of its shape, the overall results of EVs analysed are shown in Figure 4. The average size of EVs was dependent on their morphology, as has already been demonstrated (Höög and Lötvall 2015). The smallest vesicles are simple with a size of 99 ± 50 nm, oval at 166 ± 54 nm and double at

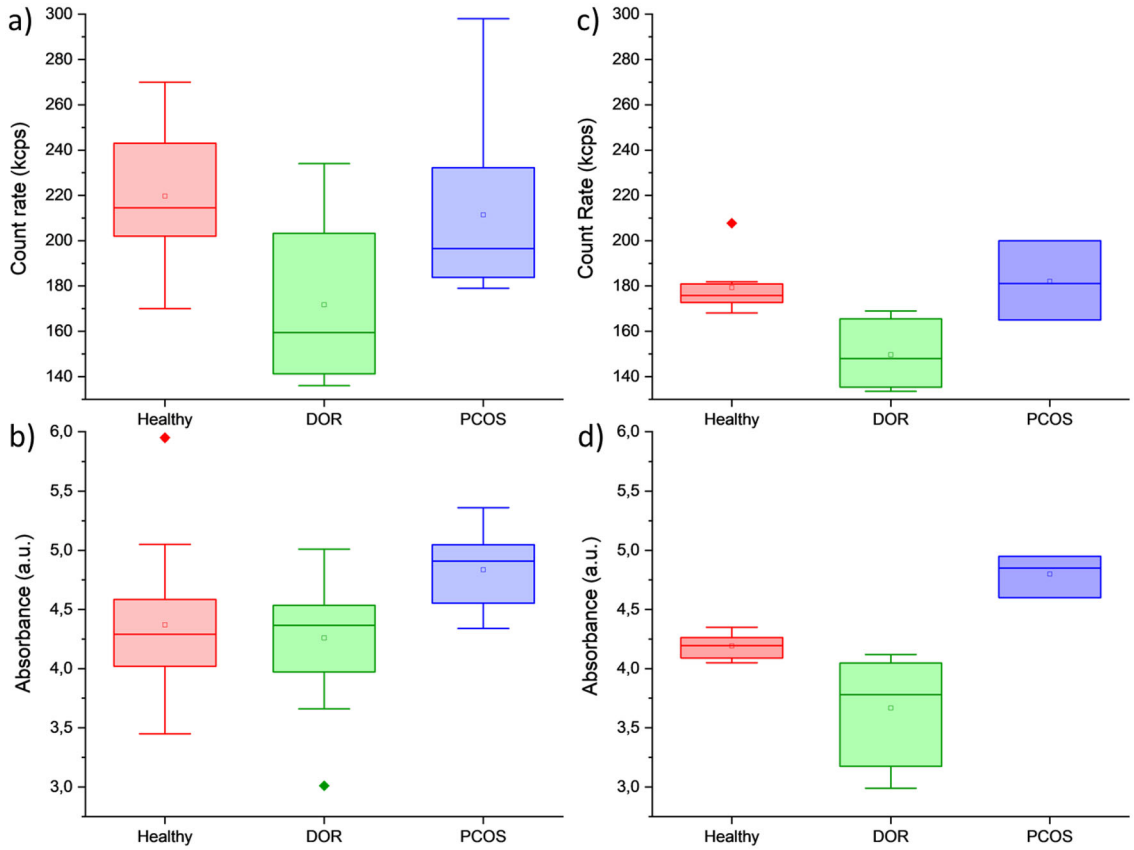

FIGURE 2 | Mean DLS count rate and absorbance at 280 nm according to the ovarian phenotype (healthy as a control, DOR or PCOS) in: (a,b) samples of individual patients (assay 1) and (c,d) pools of patients (assay 2). The square dot indicates the mean value and the horizontal bar inside the box indicates the median value.

TABLE 1 | EV's average size in function of their shape and the pathology of the subject as obtained by Cryo-TEM.

EV shape	Simple	Oval	Double
Healthy	99 nm ± 50 nm	154 nm ± 50 nm	170 nm ± 51 nm
DOR	107 nm ± 46 nm	184 nm ± 40 nm	213 nm ± 49 nm
PCOS	88 nm ± 46 nm	161 nm ± 59 nm	192 nm ± 79 nm

194 ± 73 nm, while the biggest vesicles are tubular at 310 ± 109 nm, pleomorphic at 407 ± 220 nm and sacs at 659 ± 369 nm.

However, the pathology did not impact the size of the total population of EVs as we could see in the EV size distribution obtained by Cryo-TEM images but also with DLS (Figure 5 and Figure S3). The size of the EVs for control subjects is 124 nm ± 60 nm, 163 nm ± 71 nm for DOR subjects which was slightly above the control but still in error margin and 137 nm ± 70 nm for the PCOS subjects (Figure 5).

The size of the EVs of a defined shape is not influenced by the ovarian pathology either. The morphologies analysed are simple, oval and double, as there were more than 30 EVs counted with these morphologies for all ovarian phenotypes. On average, double EVs were larger than oval EVs, which are larger than simple EVs for all ovarian phenotypes, as can be seen in Table 1 and Figure S4. Again, the size of the different shaped EVs were slightly above average for DOR subjects, which can explain the higher size for the total EV.

3.3 | MiRNA Analysis

To analyse the content of the FF-EVs, two subgroups (Large EV and Small EV) were prepared using differential UC (see Figure 1 and Table S1). The DLS data for the EV subgroups prior to miRNA analysis are presented in Figure S5. The distribution of nucleotide lengths in the RNA population purified from the EVs was first assessed using a pico RNA kit (Agilent), which allows for the qualitative detection of RNA fragments ranging from 25 to 6000 nucleotides. Gel electrophoresis of the RNA revealed that most of the RNA population was less than 200 nucleotides, with a predominant distribution around 25 nucleotides (see Figure S6). The samples displayed a typical RNA signature from EVs, as they did not show ribosomal RNA (Crescitelli et al. 2013) (see

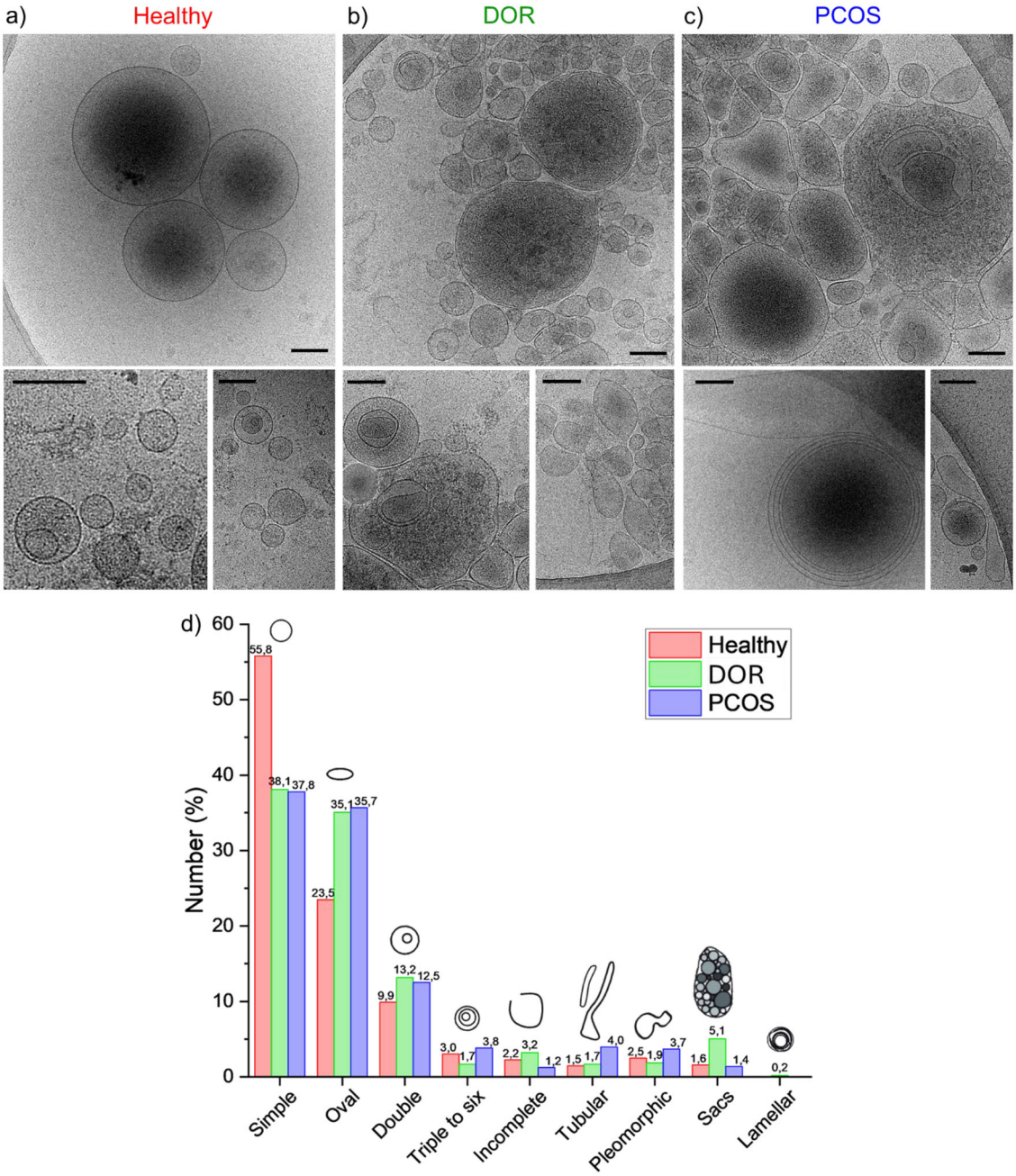

FIGURE 3 | Cryo-TEM images illustrate the diversity of size and morphologies of EVs obtained from (a) healthy individuals, (b) patients with DOR and (c) patients with PCOS. All scale bars are 100 nm. (d) A morphological analysis of EVs was conducted based on a modified classification (Höög and Lötvall 2015; Neyroud et al. 2022) for healthy individuals and infertile patients with DOR or PCOS. This analysis was performed on 215 images containing a total of two 138EVs.

Figure S7). This result indicates that the RNA content in the EVs corresponding to the three ovarian phenotypes mainly consists of small-sized RNAs under 150 nucleotides.

To further investigate the potential variations within the distribution of small RNA, the RNA population of each sample was analysed using a small RNA kit (Agilent), which facilitates qualitative analysis of RNA fragments ranging from 6 to 150 nucleotides (see Figure 6 and Figure S7). The patient's age did not significantly affect the gel profiles, as evidenced by the similarities in position, width, height and area of the peaks in both the 21–30 and 31–40 age groups (cf. Figure 6 and Figure S7). This suggests that age does not significantly influence the RNA content and fragmentation patterns within the EVs. Consequently, only the gels from the 21–30 age group are presented in Figure 6.

As shown in Figure 6, large and small EVs exhibited two distinct RNA size distribution patterns. The large EVs demonstrated a broad RNA distribution ranging from approximately 20 nucleotides (nt) to 80 nt, with an additional smaller portion of longer RNA fragments ranging from 80 to 150 nt. In contrast, the RNA size distribution in small EVs was much better defined, predominantly consisting of RNA under 80 nt. This distribution revealed a clear difference between control samples and those

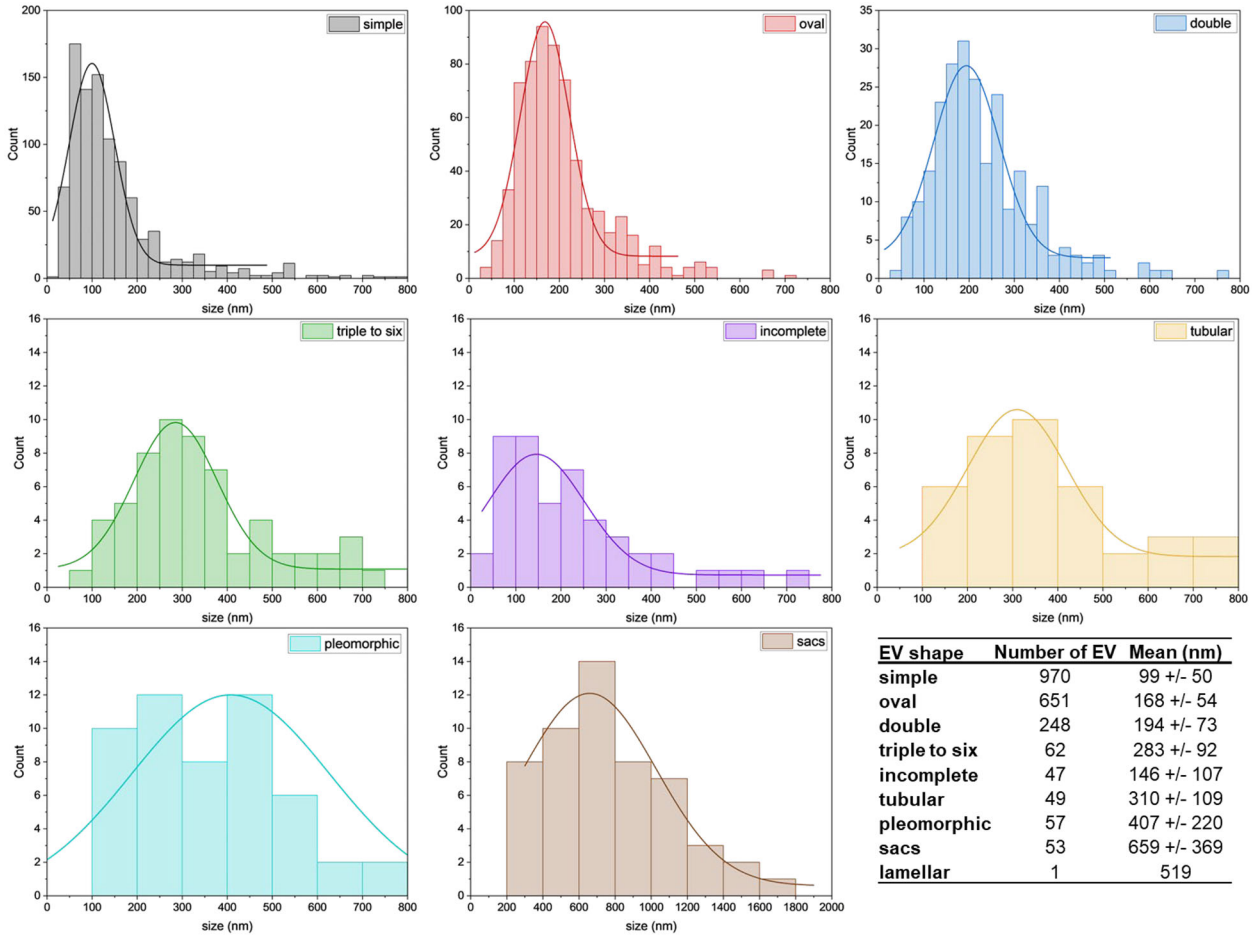

EV shape	Number of EV	Mean (nm)
simple	970	99 +/- 50
oval	651	168 +/- 54
double	248	194 +/- 73
triple to six	62	283 +/- 92
incomplete	47	146 +/- 107
tubular	49	310 +/- 109
pleomorphic	57	407 +/- 220
sacs	53	659 +/- 369
lamellar	1	519

FIGURE 4 | EV size distribution and Gauss fit in function of their morphology all ovarian phenotypes combined were obtained by Cryo-TEM analysis.

TABLE 2 | RNA concentration ([RNA] in ng/μL) in EVs from small RNA digital gel electrophoresis.

Sample fraction	Large EVs	Small EVs
Healthy	6.11	3.4 6 ± 0.17
DOR	3.44 ± 0.1	1.37 ± 0.17
PCOS	4.20 ± 0.29	1.65 ± 0.23

from infertile women (DOR or PCOS). For the healthy samples depicted in Figure 6, seven discrete and well-defined RNA bands were observed, corresponding to sizes of 18, 26, 31, 36, 44, 51 and 60 nt. In comparison, the RNA sizes in both the DOR and PCOS samples were mainly restricted to 17, 26 and 31 nt.

Therefore, the presence of well-defined RNA peaks of 36 nt or greater can be associated with healthy samples, while their absence may indicate potential ovarian dysfunction.

The RNA concentration in the various samples varied significantly depending on the ovarian phenotype. The samples from the control group, regardless of size fraction, had a higher concentration of RNA (see Table 2 and Table S3). EVs from DOR patients contained the lowest RNA content, representing only 56% of the average amount found in healthy samples. In comparison, the EVs from patients with PCOS had an RNA content of 69% of that observed in healthy samples. Notably, the fraction containing larger EVs had twice as much RNA as the fraction containing smaller EVs. However, no significant difference in RNA concentration was detected between the two age groups.

In summary, there is an overall underexpression of RNA, beyond the targeted RNA associated with ovarian dysfunction, whether it is characterized by hyperactivity or hypoactivity. This suggests a broader suppression of RNA content in EVs linked to these ovarian conditions.

Finally, the samples were sequenced using Illumina Next Generation Sequencing. We focused on miRNAs that were detected with an average of at least 10 reads per category. This analysis allowed us to identify microRNAs that were exclusively expressed in healthy patients, PCOS patients or DOR patients (see Figure 7).

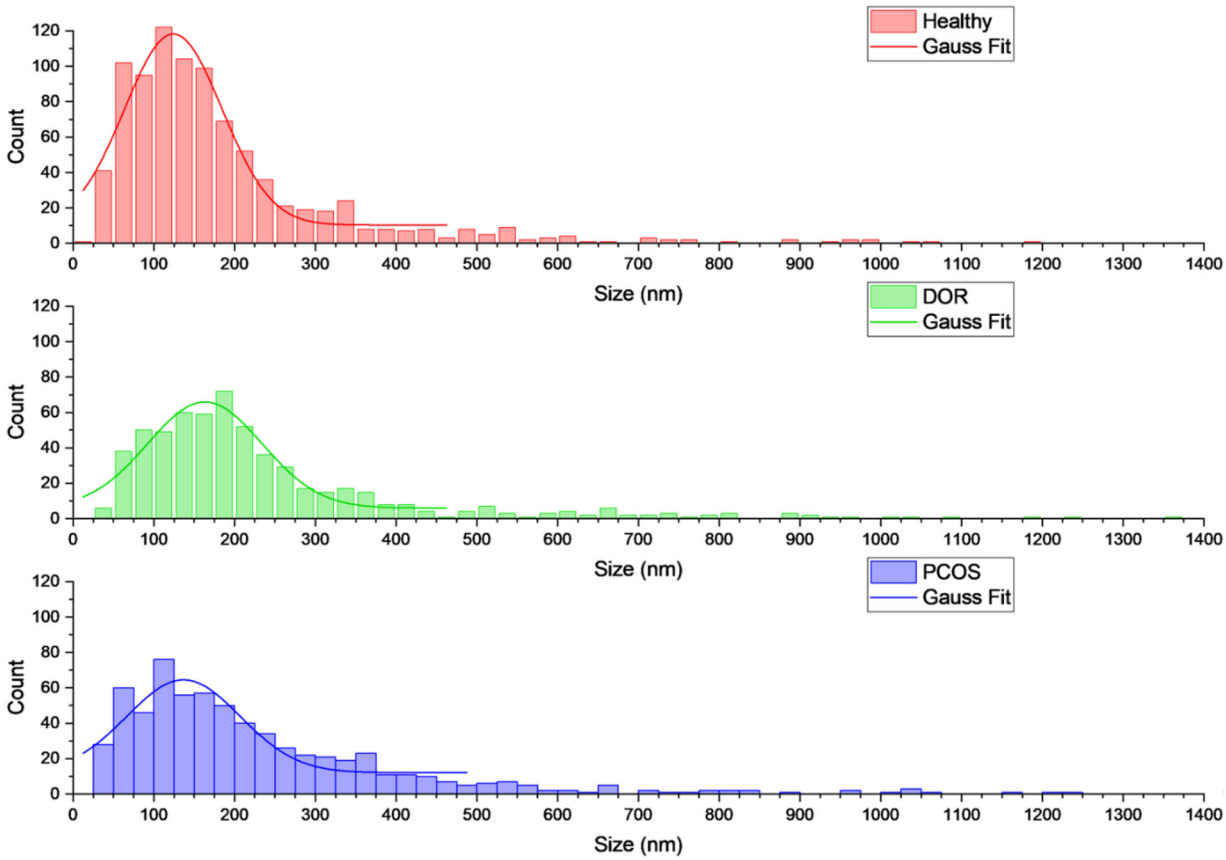

FIGURE 5 | EV's size distribution as obtained by analysis of the Cryo-TEM images.

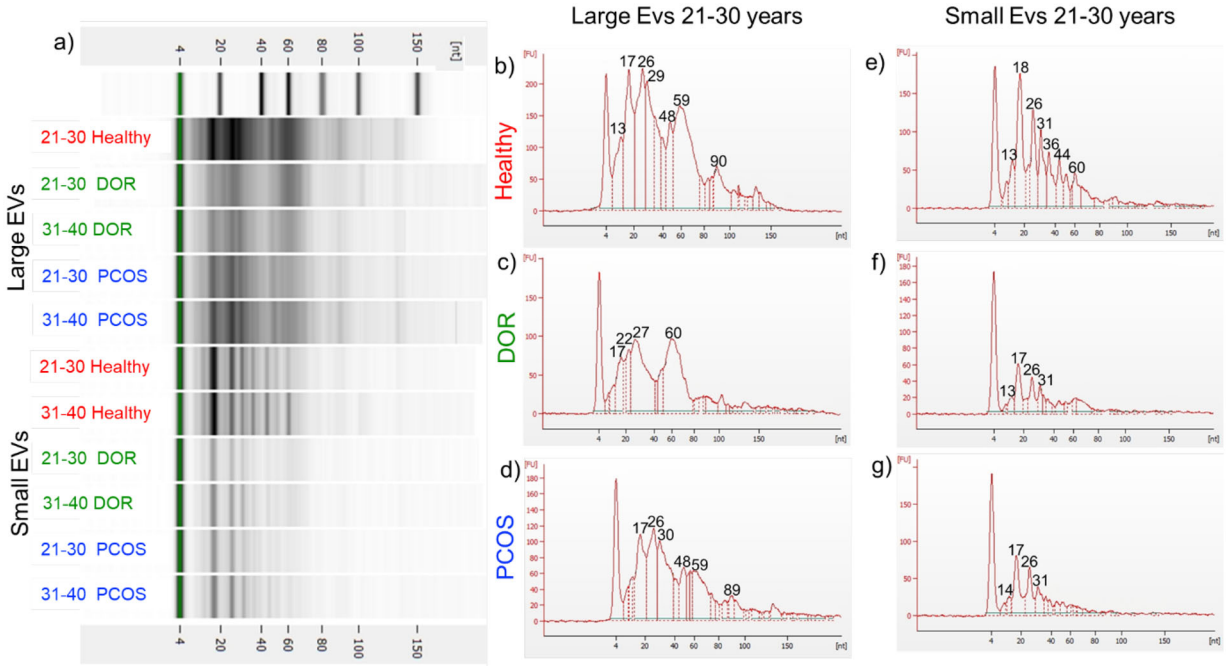

FIGURE 6 | RNA nucleotide length profile: (a) Digital electrophoresis gels of small RNA (6–150 nucleotides [nt]) found in large EVs and small EVs samples. The corresponding gel cross-section views are presented for patients aged 21–30 years in panels (b–d) large EVs and panels (e–g) small EVs.

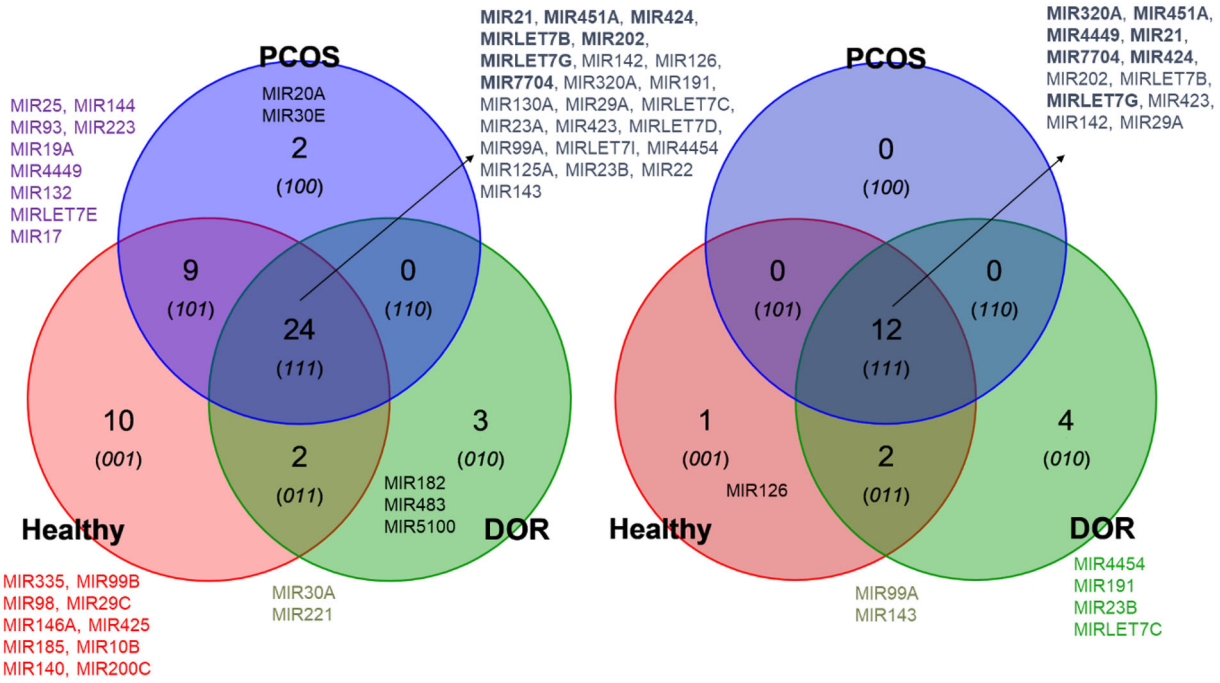

FIGURE 7 | Venn diagram of expression of miRNAs in large EVs (left) and small EVs (right). The expression values can be found in Table S4.

Among these, 23 miRNAs were present in both small and large EVs, 44 were exclusive to large EVs and one was exclusive to small EVs (refer to Figure S8 right and Table S5). Additionally, the age of the patients did not seem to influence the expression of miRNAs (see Figure S8 left and Table S6).

In large FF-EVs, we identified a total of 13 microRNAs (miRNAs) that were downregulated in both PCOS and DOR. These include miR-21, miR-let-7b, miR-126, miR-191, miR-let-7c, miR-25, miR-93, miR-19a, miR-335, miR-99b, miR-425, miR-146a and miR-185. Additionally, we found 15 miRNAs that were downregulated exclusively in DOR patients, which are miR-451a, miR-424, miR-142, miR-130a, miR-23a, miR-let-7d, miR-99a, miR-144, miR-4449, miR-223, miR-let-7e, miR-132, miR-98, miR-140 and miR-30e. We also identified seven miRNAs that were downregulated in PCOS patients: miR-29a, miR-let-7i, miR-10b, miR-200c, miR-483, miR-221 and miR-30a. In contrast, we observed one miRNA (miR-182) that was upregulated in DOR. Furthermore, there were 15 miRNAs that displayed normal regulation in both PCOS and DOR: miR-202, miR-7704, miR-let-7 g, miR-320a, miR-4454, miR-423, miR-22, miR-23b, miR-125a, miR-143, miR-17, miR-29c, miR-5100, miR-20a and ENSG00000275110.

In contrast, in the smaller FF-EVs, most miRNAs exhibited normal regulation, with the exceptions of miR-4454 and miR-23b, which were overexpressed in DOR patients, and miR-191, which was underexpressed in PCOS patients. Due to the limited number of deregulated miRNAs in small EVs, the following results will focus on the expression levels and functions of miRNAs in large EVs (refer to Figure 7 and Table S4 for additional details).

In this study, we identified miRNAs that were already found underexpressed in PCOS patients, including miR-let7i (X. Jiang et al. 2021), miR-29a (Deswal and Dang 2020), miR-200c and miR-483 (Hu et al. 2020). Some underexpressed miRNAs in PCOS patients have a proven link to fertility. For example, miR-10b inhibits granulosa cell development during folliculogenesis (Jiajie et al. 2017), and miR-200c suppresses granulosa cell proliferation (He et al. 2019). The underexpression of these miRNAs may be directly associated with follicular hyperactivity in PCOS. Similarly, miR-483 is essential for embryo development and is found to be underexpressed during pregnancy (Muraoka et al. 2024), while miR-29a is linked to positive pregnancy outcomes and is among the 20 most abundant miRNAs in the FF of good-quality oocytes (Gad et al. 2022; Scalici et al. 2016). Therefore, the underexpression of these miRNAs in the FF-EVs of PCOS patients could contribute to infertility.

Additionally, we identified miRNAs that are both underexpressed in PCOS and DOR and have been validated as markers for PCOS in previous studies. These include miR-let7c, miR-19a (Deswal and Dang 2020), miR-let7b (Scalici et al. 2016), miR-21 and miR-93 (Naji et al. 2018), miR-335 (S. Zhang et al. 2023), miR-146a (Cirillo et al. 2019), miR-25 and miR-425 (S. Jiang et al. 2021). Notably, miR-21 and miR-335 have also been reported as downregulated in the FF-EVs of DOR patients (Shen et al. 2023).

MiR-21 plays a crucial role in the development and maturation of oocytes and is underexpressed in infertile women (Jenabi et al. 2023). This underexpression of miR-21 can lead to apoptosis in granulosa cells and ovarian tissue, resulting in lower ovulation rates in mice (Carletti et al. 2010). Additionally, miRNAs from the let-7 family, such as miR-let-7b and miR-let-7c, promote embryonic development (Cao et al. 2015). MiR-191 ranks among the top 20 overexpressed miRNAs found in high-quality FF (Gad et al. 2022). MiR-126 has been shown to enhance the proliferation of granulosa cells and inhibit apoptosis in vitro in rats induced with DOR (Qu et al. 2022). Moreover, miR-335 promotes estradiol production in mice; its injection in mice with PCOS can correct hormone levels and restore fertility (S. Zhang

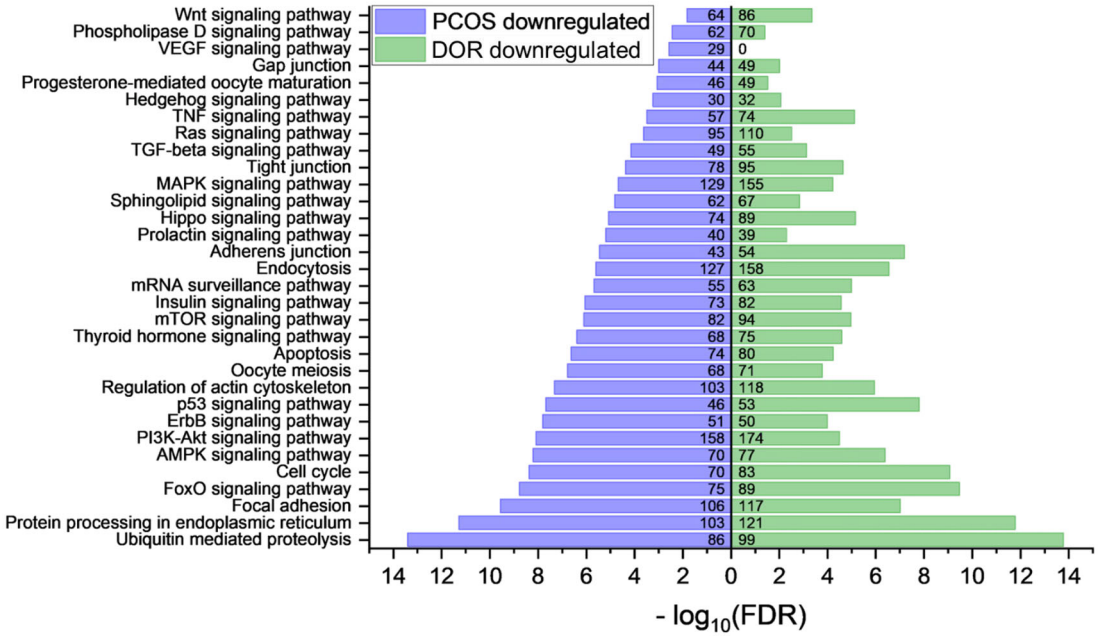

FIGURE 8 | In silico pathway analysis of downregulated miRNAs in PCOS compared to DOR conducted using DIANA miRPath-v4. Only significant results are plotted ($p < 0.05$).

et al. 2023). Downregulation of miR-320a is associated with a decreased quantity and quality of mature oocytes (Scalici et al. 2016). Finally, the expression of miR-425 is positively correlated with FF quality and enhances the development, proficiency and maturation of oocytes (Aoki et al. 2024). The underexpression of these miRNAs in both PCOS and DOR patients may contribute to poor follicular development and, consequently, infertility.

Some miRNAs are downregulated, specifically in patients presenting ovarian failure. Among these, miR-424, miR-130a and miR-let-7d have been found to be underexpressed in the FF of patients (Shen et al. 2023). Additionally, miR-424 (Du et al. 2020; Yuan et al. 2021), miR-23a (Yang et al. 2012), miR-99a (Gad et al. 2023; Geng et al. 2019), miR-144 (Donadeu et al. 2017) and miR-4449 (Wang et al. 2023) are known to regulate the proliferation and apoptosis of granulosa cells. Furthermore, miR-132 is associated with embryo quality (Machtinger et al. 2017), while miR-let-7d is overexpressed in cases of good oocyte quality (Gad et al. 2022). The dysregulation of these miRNAs may help explain why patients have fewer and lower-quality follicles, contributing to their infertility.

When comparing results with previous studies, it is essential to consider the origin of the samples, whether they come from FF, plasma or granulosa cells. The differential expression of miRNAs involved in ovarian function is influenced not only by the type of sample but also by the treatment regimen of patients undergoing IVF. It is important to note that deregulated miRNAs from different sources may exhibit opposite expression patterns. For instance, miR-21 is found to be upregulated in granulosa cells but downregulated in FF within the same group of patients (Jenabi et al. 2023; Naji et al. 2017).

Furthermore, as Scalici points out (Scalici et al. 2016), several other parameters must be considered, such as the specific IVF protocol used. The choice between agonist or antagonist IVF protocols can significantly impact miRNA expression. In our study, miR-132 and miR-320 are normo-regulated in both infertile patients (DOR and PCOS), this finding aligns with another study that employed an antagonist IVF protocol (Roth et al. 2014). However, it contrasts with the results of another team that utilized agonist IVF protocol, which found an overexpression of both miRNAs in PCOS patients (Sang et al. 2013).

Further analysis was conducted on the downregulated microRNAs in patients presenting with ovarian dysfunction using union pathway analysis to explore the target genes and dysregulated pathways. Although there were no common microRNAs identified, we found that the same signalling pathways are affected by the ovarian dysfunction phenotype. An exception is the VEGF pathway, which is crucial for angiogenesis, triggers ovulation and maintains both oocyte health and luteal vasculogenesis (Li et al. 2020; Z. Zhang et al. 2019); this pathway does not appear to be altered in patients with DOR but is affected for PCOS patients. Additionally, some pathways are less disturbed in the DOR phenotype (see Figure 8).

Further differential analysis revealed a significant difference in the types of RNA present in the fractions containing large EVs compared to those with small EVs (see Figure 8). Consistent with previous analyses, the fraction of large EVs show overexpression of several miRNAs, including miR-21, miR-93, miR-424 and miR-130A (for a complete list, refer to Table S8), indicating an enrichment of miRNAs in the large EV fraction. In contrast, certain RNAs such as vault RNAs (e.g., VTRNA1-1, VTRNA1-2), small nucleolar RNAs (e.g., SNORA57, SNORA64), and long non-coding RNAs (e.g., LINC01979, LINC02762) are underexpressed in large EVs compared to small EVs. Additionally, a few miRNAs, like miR-4449 and miR-320A, are exclusively overexpressed in the small EVs.

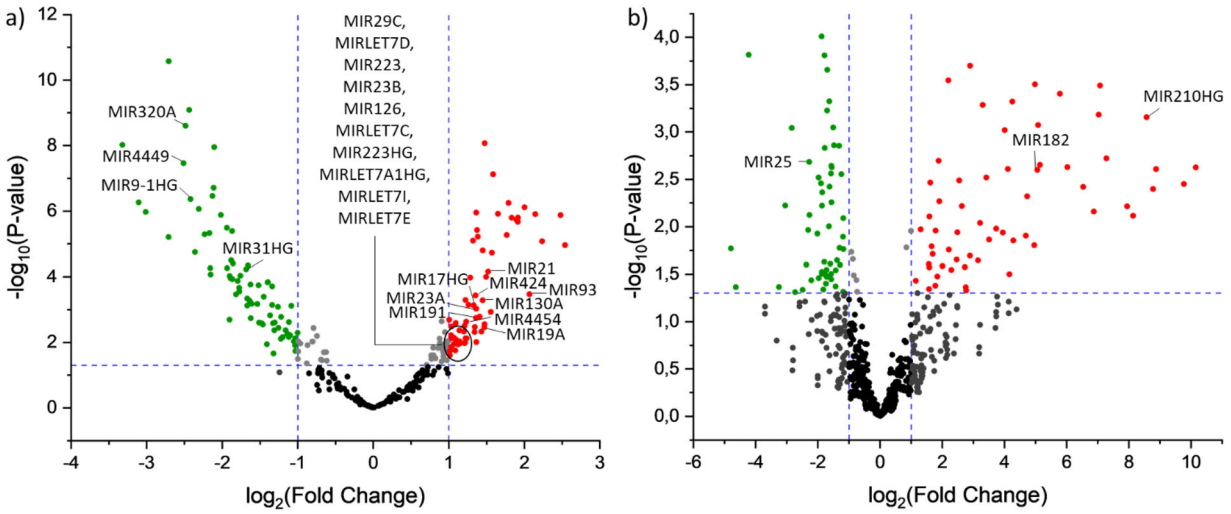

FIGURE 9 | Volcano plots of non-coding RNA sequencing results comparing: (a) Large EVs to Small EVs (refer to the complete list in Table S8) and (b) DOR patients to healthy patients (see the complete list in Table S7). The y-axis represents the negative logarithm of the *p*-value (base 10), while the x-axis shows the logarithm of the fold change (FC) (base 2). In the graph, red points indicate RNAs that are significantly overexpressed (log2FC > 1.0 and *p*-value < 0.05), while green points represent RNAs that are significantly underexpressed (log2FC < −1.0 and *p*-value < 0.05).

Our finding indicated that deregulation primarily occurs in large EVs, while miRNAs in small EVs remain normally regulated in patients with ovarian dysfunction, despite being deregulated in the large EVs from the same patients. The underexpression of miRNAs in small EVs suggests that this fraction may not be suitable for examining miRNA dysregulation.

The sequencing results indicate that certain miRNAs are significantly overexpressed in the large EV fraction of DOR patients compared to healthy individuals. Specifically, miR210HG and miR182 are found to be overexpressed, while miR25 is significantly underexpressed in cases of ovarian hypoactivity (Cf. Figure 9). Interestingly, the opposite trends have been reported in cases of ovarian hyperactivity, such as PCOS, where miR-182 is underexpressed (Naji et al. 2018) and miR-25 is overexpressed (Hu et al. 2020). Detailed sequencing results can be found in Tables S7 and S8.

4 | Conclusion

In conclusion, we noted differences in protein content among patients with ovarian dysfunction. Specifically, patients with PCOS had higher protein content than average, while patients with DOR had lower concentrations. Although the size of FF-EVs did not vary, there were differences in both the concentration and polydispersity of the crude FF-EVs, as observed through DLS. The morphology of FF-EVs is influenced by ovarian dysfunction. In particular, FF-EVs of infertile patients display less rounded and more complex shapes. In addition to these morphological differences between conditions, there is a considerable variation in the non-coding RNA content of EVs, particularly in miRNAs. Infertile patients tend to exhibit lower miRNA concentration and appear to lose the distinct signature of RNA diversity, as indicated by the electrophoresis digital gels. RNA sequencing further revealed miRNA dysregulation in both DOR and PCOS patients compared to healthy controls. Notably, there is a significant overexpression of miR-210HG and miR-182, while miR-25 is significantly underexpressed in DOR patients relative to controls.

Pathway analysis involving the deregulated miRNAs and their target genes in PCOS and DOR patients is crucial for considering the therapeutic applications of miRNAs. This study is the first to characterize and correlate EV morphologies, their physical properties and miRNA content in healthy patients compared to those with ovarian dysfunction resulting in infertility. Thus, these findings enhance our understanding of the molecular signatures related to ovarian diseases but also highlight the potential for the management of ovarian disorders, representing a significant advance in reproductive healthcare.

Author Contributions

Solène Ducarre: data curation (equal), investigation (equal), writing–original draft (equal). **Regina Maria Chiechio**: data curation (equal), formal analysis (equal), writing–original draft (equal). **Gregory Moulin**: data curation (equal), formal analysis (equal). **Ester Butera**: data curation (equal), writing–review and editing (equal). **Aurélien Dupont**: software (equal), visualization (equal). **Christophe Penno**: formal analysis (equal), validation (equal), writing–review and editing (equal). **Abdelhak El Amrani**: validation (equal), writing–review and editing (equal). **Claire Heichette**: investigation (equal), supervision (equal). **Pascale Even-Hernandez**: data curation (equal), formal analysis (equal), validation (equal), writing–review and editing (equal). **Valerie Marchi**: conceptualization (equal), data curation (equal), formal analysis (equal), methodology (equal), writing–review and editing (equal). **Célia Ravel**: conceptualization (equal), formal analysis (equal), methodology (equal), supervision (equal), writing–review and editing (equal).

Conflicts of Interest

The authors declare no conflicts of interest.

Data Availability Statement

The data that supports the findings of this study are available in the supplementary material of this article.

References

Aitken, R. J. 2024. "Population Decline: Where Demography, Social Science, and Biology Intersect." *Reproduction (Cambridge, England)* 168, no. 1: https://doi.org/10.1530/REP-24-0070.

Aoki, S., Y. Inoue, S. Hara, J. Itou, K. Shirasuna, and H. Iwata. 2024. "microRNAs Associated With the Quality of Follicular Fluids Affect Oocyte and Early Embryonic Development." *Reproductive Medicine and Biology* 23, no. 1: e12559. https://doi.org/10.1002/rmb2.12559.

Azziz, R., E. Carmina, Z. I. J. Chen, et al. 2016. "Polycystic Ovary Syndrome." *Nature Reviews Disease Primers* 2, no. 1: 1–18. https://doi.org/10.1038/nrdp.2016.57.

Cao, R., W. J. Wu, X. L. Zhou, P. Xiao, Y. I. Wang, and H. L. Liu. 2015. "Expression and Preliminary Functional Profiling of the Let-7 Family During Porcine Ovary Follicle Atresia." *Molecules and Cells* 38, no. 4: 304–311. https://doi.org/10.14348/molcells.2015.2122.

Carletti, M. Z., S. D. Fiedler, and L. K. Christenson. 2010. "MicroRNA 21 Blocks Apoptosis in Mouse Periovulatory Granulosa Cells1." *Biology of Reproduction* 83, no. 2: 286–295. https://doi.org/10.1095/biolreprod.109.081448.

Cedars, M. I. 2022. "Evaluation of Female Fertility-AMH and Ovarian Reserve Testing." *Journal of Clinical Endocrinology and Metabolism* 107, no. 6: 1510–1519. https://doi.org/10.1210/clinem/dgac039.

Cirillo, F., C. Catellani, P. Lazzeroni, et al. 2019. "MiRNAs Regulating Insulin Sensitivity Are Dysregulated in Polycystic Ovary Syndrome (PCOS) Ovaries and Are Associated With Markers of Inflammation and Insulin Sensitivity." *Frontiers in Endocrinology* 10: 879. https://doi.org/10.3389/fendo.2019.00879.

Cohen, J., N. Chabbert-Buffet, and E. Darai. 2015. "Diminished Ovarian Reserve, Premature Ovarian Failure, Poor Ovarian Responder – A Plea for Universal Definitions." *Journal of Assisted Reproduction and Genetics* 32, no. 12: 1709–1712. https://doi.org/10.1007/s10815-015-0595-y.

Crescitelli, R., C. Lässer, T. G. Szabó, et al. 2013. "Distinct RNA Profiles in Subpopulations of Extracellular Vesicles: Apoptotic Bodies, Microvesicles and Exosomes." *Journal of Extracellular Vesicles* 2, no. 1. https://doi.org/10.3402/jev.v2i0.20677.

Deswal, R., and A. S. Dang. 2020. "Dissecting the Role of Micro-RNAs as a Diagnostic Marker for Polycystic Ovary Syndrome: A Systematic Review and Meta-Analysis." *Fertility and Sterility* 113, no. 3: 661–669.e2. https://doi.org/10.1016/j.fertnstert.2019.11.001.

Donadeu, F. X., S. D. Sontakke, and J. Ioannidis. 2017. "MicroRNA Indicators of Follicular Steroidogenesis." *Reproduction, Fertility and Development* 29, no. 5: 906–912. https://doi.org/10.1071/RD15282.

Du, J., X. Lin, R. Wu, et al. 2020. "miR-424 Suppresses Proliferation and Promotes Apoptosis of human Ovarian Granulosa Cells by Targeting Apelin and APJ Expression." *American Journal of Translational Research* 12, no. 7: 3660–3673.

Dubochet, J., M. Adrian, J.-J. U. Chang, et al. 1988. "Cryo-Electron Microscopy of Vitrified Specimens." *Quarterly Reviews of Biophysics* 21, no. 2: 129–228. https://doi.org/10.1017/S0033583500004297.

Ehrmann, D. A. 2005. "Polycystic Ovary Syndrome." *New England Journal of Medicine* 352, no. 12: 1223–1236. https://doi.org/10.1056/NEJMra041536.

Ferraz A. M. M., M. de, M. Fujihara, et al. 2020. "Follicular Extracellular Vesicles Enhance Meiotic Resumption of Domestic Cat Vitrified Oocytes." *Scientific Reports* 10, no. 1: 8619. https://doi.org/10.1038/s41598-020-65497-w.

Gad, A., K. Joyce, N. G. Menjivar, et al. 2023. "Extracellular Vesicle-microRNAs Mediated Response of Bovine Ovaries to Seasonal Environmental Changes." *Journal of Ovarian Research* 16, no. 1: 101. https://doi.org/10.1186/s13048-023-01181-7.

Gad, A., M. Murin, A. Bartkova, et al. 2022. "Small-Extracellular Vesicles and Their microRNA Cargo From Porcine Follicular Fluids: The Potential Association With Oocyte Quality." *Journal of Animal Science and Biotechnology* 13, no. 1: 82. https://doi.org/10.1186/s40104-022-00723-1.

Geng, Y., C. Sui, Y. Xun, Q. Lai, and L. Jin. 2019. "MiRNA-99a Can Regulate Proliferation and Apoptosis of Human Granulosa Cells via Targeting IGF-1R in Polycystic Ovary Syndrome." *Journal of Assisted Reproduction and Genetics* 36, no. 2: 211–211. https://doi.org/10.1007/s10815-018-1335-x.

Goodman, N. F., R. H. Cobin, W. Futterweit, et al. 2015a. "American Association of Clinical Endocrinologists, American College of Endocrinology, and Androgen Excess and PCOS Society Disease State Clinical Review: Guide to the Best Practices in the Evaluation and Treatment of Polycystic Ovary Syndrome—Part 1." *Endocrine Practice* 21, no. 11: 1291–1300. https://doi.org/10.4158/EP15748.DSC.

Goodman, N. F., R. H. Cobin, W. Futterweit, et al. 2015b. "American Association of Clinical Endocrinologists, American College of Endocrinology, and Androgen Excess and PCOS Society Disease State Clinical Review: Guide to the Best Practices in the Evaluation and Treatment of Polycystic Ovary Syndrome—Part 2." *Endocrine Practice* 21, no. 12: 1415–1426. https://doi.org/10.4158/EP15748.DSCPT2.

He, T., Y. Sun, Y. Zhang, et al. 2019. "MicroRNA-200b and microRNA-200c Are Up-Regulated in PCOS Granulosa Cell and Inhibit KGN Cell Proliferation Via Targeting PTEN." *Reproductive Biology and Endocrinology* 17, no. 1: 68. https://doi.org/10.1186/s12958-019-0505-8.

Höög, J. L., and J. Lötvall. 2015. "Diversity of Extracellular Vesicles in Human Ejaculates Revealed by Cryo-Electron Microscopy." *Journal of Extracellular Vesicles* 4, no. 1: 28680. https://doi.org/10.3402/jev.v4.28680.

Hu, J., T. Tang, Z. Zeng, J. Wu, X. Tan, and J. Yan. 2020. "The Expression of Small RNAs in Exosomes of Follicular Fluid Altered in Human Polycystic Ovarian Syndrome." *PeerJ* 8, no. février:e8640. https://doi.org/10.7717/peerj.8640.

Jenabi, M., P. Khodarahmi, F. Tafvizi, and S. Z. Bostanabad. 2023. "Evaluation of the Potential of miR-21 as a Diagnostic Marker for Oocyte Maturity and Embryo Quality in Women Undergoing ICSI." *Scientific Reports* 13, no. 1: 1440. https://doi.org/10.1038/s41598-023-28686-x.

Jiajie, T. U., Y. Yanzhou, A. Cheung Hoi-Hung, C. Zi-Jiang, and C. Wai-Yee. 2017. "Conserved miR-10 Family Represses Proliferation and Induces Apoptosis in Ovarian Granulosa Cells." *Scientific Reports* 7, no. 1: 41304. https://doi.org/10.1038/srep41304.

Jiang, S., Q. Li, C. Wang, Y. Pang, Z. Sun, and R. Xiao. 2021. "In Situ Exosomal MicroRNA Determination by Target-Triggered SERS and Fe_3O_4@TiO_2 – Based Exosome Accumulation" *ACS Sensors* 6, no. 3: 852–862. https://doi.org/10.1021/acssensors.0c01900.

Jiang, X., J. Li, B. Zhan, et al. 2021. "Differential Expression Profile of Plasma Exosomal microRNAs in Women With Polycystic Ovary Syndrome." *Fertility and Sterility* 115, no. 3: 782–792. https://doi.org/10.1016/j.fertnstert.2020.08.019.

Joham, A. E., R. J. Norman, E. Stener-Victorin, et al. 2022. "Polycystic Ovary Syndrome." *Lancet Diabetes & Endocrinology* 10, no. 9: 668–680. https://doi.org/10.1016/S2213-8587(22)00163-2.

Li, C., Z. Liu, W. Li, et al. 2020. "The FSH–HIF-1α–VEGF Pathway Is Critical for Ovulation and Oocyte Health but Not Necessary for Follicular Growth in Mice" *Endocrinology* 161, no. 4: bqaa038. https://doi.org/10.1210/endocr/bqaa038.

Lischnig, A., M. Bergqvist, T. Ochiya, and C. Lässer. 2022. "Quantitative Proteomics Identifies Proteins Enriched in Large and Small Extracellular Vesicles." *Molecular & Cellular Proteomics* 21, no. 9: 100273. https://doi.org/10.1016/j.mcpro.2022.100273.

Macaulay, A. D., I. Gilbert, J. Caballero, et al. 2014. "The Gametic Synapse: RNA Transfer to the Bovine Oocyte1." *Biology of Reproduction* 91, no. 4: 90. https://doi.org/10.1095/biolreprod.114.119867.

Machtinger, R., R. S. Rodosthenous, M. Adir, et al. 2017. "Extracellular microRNAs in Follicular Fluid and Their Potential Association With Oocyte Fertilization and Embryo Quality: An Exploratory Study." *Journal of Assisted Reproduction and Genetics* 34, no. 4: 525–533. https://doi.org/10.1007/s10815-017-0876-8.

Mimouni, N. El. H., I. Paiva, A.-L. Barbotin, et al. 2021. "Polycystic Ovary Syndrome Is Transmitted via a Transgenerational Epigenetic Process." *Cell Metabolism* 33, no. 3: 513–530. e8. https://doi.org/10.1016/j.cmet.2021.01.004.

Muraoka, A., A. Yokoi, K. Yoshida, et al. 2024. "Small Extracellular Vesicles in Follicular Fluids for Predicting Reproductive Outcomes in Assisted Reproductive Technology." *Communications Medicine* 4, no. 1: 1–9. https://doi.org/10.1038/s43856-024-00460-8.

Naji, M., A. Aleyasin, S. Nekoonam, E. Arefian, R. Mahdian, and F. Amidi. 2017. "Differential Expression of miR-93 and miR-21 in Granulosa Cells and Follicular Fluid of Polycystic Ovary Syndrome Associating With Different Phenotypes." *Scientific Reports* 7, no. 1: 14671. https://doi.org/10.1038/s41598-017-13250-1.

Naji, M., S. Nekoonam, A. Aleyasin, et al. 2018. "Expression of miR-15a, miR-145, and miR-182 in Granulosa-Lutein Cells, Follicular Fluid, and Serum of Women With Polycystic Ovary Syndrome (PCOS)." *Archives of Gynecology and Obstetrics* 297, no. 1: 221–231. https://doi.org/10.1007/s00404-017-4570-y.

Neyroud, A.-S., R. M. Chiechio, G. Moulin, et al. 2022. "Diversity of Extracellular Vesicles in Human Follicular Fluid: Morphological Analysis and Quantification." *International Journal of Molecular Sciences* 23, no. 19: 11676. https://doi.org/10.3390/ijms231911676.

Penzias, A., R. Azziz, K. Bendikson, et al. 2020. "Testing and Interpreting Measures of Ovarian Reserve: A Committee Opinion." *Fertility and Sterility* 114, no. 6: 1151–1157. https://doi.org/10.1016/j.fertnstert.2020.09.134.

Qu, Q., L. Liu, Y. Cui, et al. 2022. "miR-126-3p Containing Exosomes Derived From human Umbilical Cord Mesenchymal Stem Cells Promote Angiogenesis and Attenuate Ovarian Granulosa Cell Apoptosis in a Preclinical Rat Model of Premature Ovarian Failure." *Stem Cell Research & Therapy* 13, no. 1: 352. https://doi.org/10.1186/s13287-022-03056-y.

Ravel, C., N. Kazdar, and J. Leveque. 2016. "Fertilité et Insuffisance Ovarienne: De Nouveaux Traitements en Perspective ?" *Gynécologie Obstétrique & Fertilité* 44, no. 1: 56–62. https://doi.org/10.1016/j.gyobfe.2015.10.008.

Roth, L. W., B. McCallie, and R. Alvero, et al. 2014. "Altered microRNA and Gene Expression in the Follicular Fluid of Women With Polycystic Ovary Syndrome." *Journal of Assisted Reproduction and Genetics* 31, no. 3: 355–362. https://doi.org/10.1007/s10815-013-0161-4.

Sang, Q., Z. Yao, H. Wang, et al. 2013. "Identification of MicroRNAs in Human Follicular Fluid: Characterization of MicroRNAs That Govern Steroidogenesis In Vitro and Are Associated with Polycystic Ovary Syndrome in Vivo." *Journal of Clinical Endocrinology & Metabolism* 98, no. 7: 3068–3079. https://doi.org/10.1210/jc.2013-1715.

Scalici, E., S. Traver, T. Mullet, et al. 2016. "Circulating microRNAs in Follicular Fluid, Powerful Tools to Explore In Vitro Fertilization Process." *Scientific Reports* 6, no. 1: 24976. https://doi.org/10.1038/srep24976.

Shen, K.-Y., X.-L. I. Dai, S. Li, et al. 2023. "Specific Expression Profile of Follicular Fluid-Derived Exosomal microRNAs in Patients With Diminished Ovarian Reserve." *BMC Medical Genomics* 16, no. 1: 308. https://doi.org/10.1186/s12920-023-01756-9.

Théry, C., K. W. Witwer, E. Aikaw, et al. 2018. "Minimal Information for Studies of Extracellular Vesicles 2018 (MISEV2018): A Position Statement of the International Society for Extracellular Vesicles and Update of the MISEV2014 Guidelines." *Journal of Extracellular Vesicles* 7, no. 1: 1535750. https://doi.org/10.1080/20013078.2018.1535750.

Wang, M., Y. Sun, D. Yuan, S. Yue, and Z. Yang. 2023. "Follicular Fluid Derived Exosomal miR-4449 Regulates Cell Proliferation and Oxidative Stress by Targeting KEAP1 in Human Granulosa Cell Lines KGN and COV434." *Experimental Cell Research* 430, no. 2: 113735. https://doi.org/10.1016/j.yexcr.2023.113735.

Welsh, J. A., D. C. I. Goberdhan, L. O'Driscoll, et al. 2024. "Minimal Information for Studies of Extracellular Vesicles (MISEV2023): From Basic to Advanced Approaches." *Journal of Extracellular Vesicles* 13, no. 2: e12404. https://doi.org/10.1002/jev2.12404.

Yang, X., Y. Zhou, S. Peng, et al. 2012. "Differentially Expressed Plasma microRNAs in Premature Ovarian Failure Patients and the Potential Regulatory Function of Mir-23a in Granulosa Cell Apoptosis." *Reproduction (Cambridge, England)* 144, no. 2: 235–244. https://doi.org/10.1530/REP-11-0371.

Yefimova, M. G., C. Lefevre, A. Bashamboo, et al. 2020. "Granulosa Cells Provide Elimination of Apoptotic Oocytes Through Unconventional Autophagy-Assisted Phagocytosis." *Human Reproduction* 35, no. 6: 1346–1362. https://doi.org/10.1093/humrep/deaa097.

Yuan, D., J. Luo, Y. Sun, L. Hao, J. Zheng, and Z. Yang. 2021. "PCOS Follicular Fluid Derived Exosomal miR-424-5p Induces Granulosa Cells Senescence by Targeting CDCA4 Expression." *Cellular Signalling* 85, no. September: 110030. https://doi.org/10.1016/j.cellsig.2021.110030.

Zhang, S., Y. Liu, M. Wang, et al. 2023. "Role and Mechanism of miR-335-5p in the Pathogenesis and Treatment of Polycystic Ovary Syndrome." *Translational Research* 252, no. février: 64–78. https://doi.org/10.1016/j.trsl.2022.07.007.

Zhang, Z., Y. Huang, J. Zhang, Z. Liu, Q. Lin, and Z. Wang. 2019. "Activation of NF-κB Signaling Pathway During HCG-Induced VEGF Expression in Luteal Cells." *Cell Biology International* 43, no. 3: 344–349. https://doi.org/10.1002/cbin.11090.

Zhao, Y., S. Pan, Y. Li, and X. Wu. 2022. "Exosomal miR-143-3p Derived From Follicular Fluid Promotes Granulosa Cell Apoptosis by Targeting BMPR1A in Polycystic Ovary Syndrome." *Scientific Reports* 12, no. 1: 4359. https://doi.org/10.1038/s41598-022-08423-6.

Supporting Information

Additional supporting information can be found online in the Supporting Information section.